Papaverine and its derivatives radiosensitize solid tumors by inhibiting mitochondrial metabolism

Martin Benej[a,b], Xiangqian Hong[c], Sandip Vibhute[d], Sabina Scott[a,b], Jinghai Wu[a,b], Edward Graves[e], Quynh-Thu Le[e], Albert C. Koong[f], Amato J. Giaccia[e], Bing Yu[c], Ching-Shih Chen[d,1], Ioanna Papandreou[a,b], and Nicholas C. Denko[a,b,2]

[a]Department of Radiation Oncology, Wexner Medical Center, The Ohio State University, Columbus, OH 43210; [b]Comprehensive Cancer Center, James Cancer Hospital and Solove Research Institute, The Ohio State University, Columbus, OH 43210; [c]Department of Biomedical Engineering, Marquette University, Milwaukee, WI 53233; [d]Department of Medicinal Chemistry School of Pharmacy, Ohio State University, Columbus, OH 43210; [e]Department of Radiation Oncology, Stanford University School of Medicine, Stanford, CA 94305; and [f]Department of Radiation Oncology, MD Anderson Cancer Center, Houston, TX 77030

Edited by Gregg L. Semenza, Johns Hopkins University School of Medicine, Baltimore, MD, and approved August 10, 2018 (received for review May 24, 2018)

Tumor hypoxia reduces the effectiveness of radiation therapy by limiting the biologically effective dose. An acute increase in tumor oxygenation before radiation treatment should therefore significantly improve the tumor cell kill after radiation. Efforts to increase oxygen delivery to the tumor have not shown positive clinical results. Here we show that targeting mitochondrial respiration results in a significant reduction of the tumor cells' demand for oxygen, leading to increased tumor oxygenation and radiation response. We identified an activity of the FDA-approved drug papaverine as an inhibitor of mitochondrial complex I. We also provide genetic evidence that papaverine's complex I inhibition is directly responsible for increased oxygenation and enhanced radiation response. Furthermore, we describe derivatives of papaverine that have the potential to become clinical radiosensitizers with potentially fewer side effects. Importantly, this radiosensitizing strategy will not sensitize well-oxygenated normal tissue, thereby increasing the therapeutic index of radiotherapy.

hypoxia | metabolism | mitochondria | radiosensitization

Hypoxia is a common microenvironmental feature of solid tumors (1) that exists because the supply of oxygen is insufficient to meet the metabolic demand of the tumor (2, 3). The poorly formed tumor blood vessels make it difficult to therapeutically increase oxygen delivery to reduce hypoxia (4). It was recognized more than six decades ago that hypoxia is a barrier to effective radiation therapy (5). This represents a serious clinical problem, as more than 50% of tumors receive radiation therapy as a part of their treatment (6).

Molecular oxygen is an electrophile that fixes radiation-induced DNA damage (7, 8), enhancing toxicity by 2.5-fold (9). Reducing tumor hypoxia before radiotherapy should therefore enhance radiation efficacy without increasing toxicity in well-oxygenated normal tissue. Previous strategies to alleviate tumor hypoxia have been primarily aimed at increasing the oxygen delivery into the tumor (10, 11). However, the restricted functionality of tumor vasculature has proven to be a major limitation for translation into the clinics.

An alternative strategy to increase tumor oxygenation is by decreasing tumor demand for oxygen through inhibition of mitochondrial respiration (12). Computational models have predicted that reducing the rate of oxygen consumption (OCR) will decrease the hypoxic fraction more effectively than increasing the rate of delivery (13). Although several drugs have been recently proposed for this purpose (14), their translational potential is limited by the requirements for uptake, the biological half-life of the compound, the toxicity due to side effects, or by the requirements for driver mutations that limit applicability to specific subgroups of cancers. An optimal drug would have universal OCR inhibition, rapid uptake without need for carrier proteins, short half-life, good safety profile, and quick clearance from the patient.

We present data here showing that the FDA-approved drug papaverine is an ideal agent for the metabolic radiosensitization of hypoxic tumors (15). Papaverine is an ergot alkaloid first isolated in 1848 (16) from *Papaver somniferum*. Papaverine does not have narcotic properties, but was used as a smooth muscle relaxant for the treatment of vasospasm and erectile dysfunction (17, 18). Its vascular effects were thought to be due to its activity as a phosphodiesterase 10A inhibitor (19). The most common adverse effects associated with long-term use include injection site fibrosis. We found that papaverine has an "off-target effect" that reversibly inhibits mitochondrial complex I in all cell lines tested. In vivo, at FDA-approved doses, papaverine increases model tumor oxygenation within 30 min and significantly enhances tumor response to RT. Genetic analysis shows that papaverine radiosensitizes through inhibition of mitochondrial function. Medicinal chemistry also shows that it is possible to molecularly separate papaverine's classical activity as a phosphodiesterase 10A (PDE10A) inhibitor from the newly recognized activity as a mitochondrial C1 inhibitor. Papaverine (PPV) derivatives that inhibit complex I without inhibiting PDE10A are a potential class of radiosensitizing drugs with fewer side effects.

Results

Papaverine Reduces OCR by Inhibiting Mitochondrial Complex I. Papaverine (PPV) was recently found to slow the growth of cells in media containing only galactose as a carbon source (20), which

Significance

Oxygen tension plays a critical role in the response to radiation therapy (RT). Here we show that hypoxic tumors can be sensitized to RT by targeting mitochondrial respiration. We identified the 150-year-old FDA-approved drug papaverine as a mitochondrial complex I inhibitor. A single dose of the drug prior to RT alleviates hypoxia in model tumors and strikingly enhances the response to RT. Well-oxygenated normal tissues are not radiosensitized. Removal of papaverine's phosphodiesterase 10A inhibitory activity by structural modification has identified potentially safer generation of complex I-inhibiting radiosensitizers.

Author contributions: E.G., Q.-T.L., A.C.K., A.J.G., S.-C.C., and N.C.D. designed research; M.B., X.H., S.V., S.S., J.W., and I.P. performed research; X.H. and B.Y. contributed new reagents/analytic tools; M.B., S.V., J.W., E.G., Q.-T.L., A.C.K., A.J.G., S.-C.C., I.P., and N.C.D. analyzed data; and M.B. and N.C.D. wrote the paper.

The authors declare no conflict of interest.

This article is a PNAS Direct Submission.

See Commentary on page 10548.

[1]Present address: Institute of New Drug Development, China Medical University, Taichung 404, Taiwan.

[2]To whom correspondence should be addressed. Email: nicholas.denko@osumc.edu.

This article contains supporting information online at www.pnas.org/lookup/suppl/doi:10.1073/pnas.1808945115/-/DCSupplemental.

Published online September 10, 2018.

indicates inhibition of mitochondrial function. We tested PPV in vitro in a panel of 28 cancer and normal cell lines and found it could decrease mitochondrial function in all cells tested in minutes at low micromolar concentrations (Fig. 1*A* and *SI Appendix*, Table S1). To determine its mechanism of action, we tested PPV in combination with established mitochondrial poisons and found it could dose-dependently block the activity of the classical complex I inhibitor rotenone (Fig. 1*B*), suggesting some competition of the two drugs. In a similar assay with other complex I inhibitors piericidin A, or capsaicin, there was no interaction (*SI Appendix*, Fig. S1 *A* and *B*). This suggests that PPV may bind to the rotenone site or possibly that its binding blocks this site, in agreement with published data (21). To confirm that PPV inhibits complex I, we treated permeabilized EO771 cells with either PPV or rotenone followed by complex II substrate succinate that can bypass complex I inhibition. Fig. 1*C* shows that succinate rescued the OCR of both rotenone and PPV-treated cells, but not that of cells treated with the complex 3 inhibitor antimycin A, confirming that PPV action is upstream of complex 2 (Fig. 1*C*).

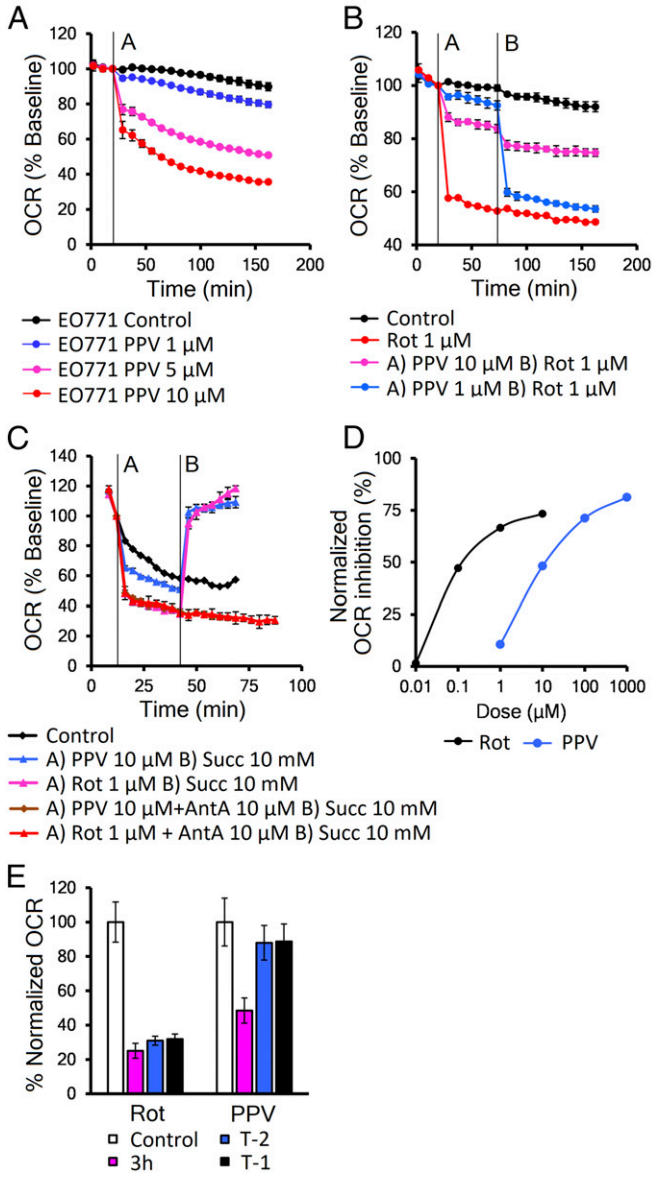

Fig. 1. Papaverine reduces OCR by inhibition of mitochondrial complex I. (*A*) Representative Seahorse data showing decreased OCR in EO771 cells. (*B*) Competition assay between papaverine and rotenone injected as indicated in EO771 cells. (*C*) Succinate rescue assay in permeabilized EO771 cells. PPV or rotenone were injected alone or in combination with complex III inhibitor antimycin A (AntA) at time A; succinate (Succ) was injected at time B. (*D*) Dose–response analysis in A549 cell line. (*E*) Drug washout experiment in A549 cells, the OCR reduction at 3 h of 10 μM PPV or 1 μM rotenone (*magenta*), and after removal at T-2 h (*blue*) or 1 h (*black*). Error bars represent SD.

To evaluate PPV's efficiency as a complex I inhibitor, we treated A549 cells with increasing doses of PPV and rotenone. Dose–response analysis shows that that PPV's IC50 for OCR is ~100× higher than rotenone's (Fig. 1*D*). We also compared the effect of PPV to other drugs suggested for use as metabolic radiosensitizers, metformin and atovaquone (*SI Appendix*, Fig. S1*C*). In vitro Seahorse analysis showed that while PPV and atovaquone took 30 min (Fig. 1*A*), metformin required 24 h (in mM concentrations) to reach full mitochondrial inhibition. Ideal metabolic radiosensitizers should have reversible activity so that potential for toxicity will be limited. Interestingly, PPV's mitochondrial effect is reversible in vitro, in comparison with the potentially more toxic irreversible effects of rotenone (22) and atovaquone. In drug washout experiments, PPV-treated cells returned to baseline OCR in less than 1 h, while rotenone- and atovaquone-treated cells showed no restoration in mitochondrial function after 3 h. This property may explain papaverine's excellent safety profile (15) (Fig. 1*E* and *SI Appendix*, Fig. S1*D*). In support of its safety, we observed no cellular toxicity in cells treated with PPV in either normoxia or hypoxia (*SI Appendix*, Fig. S1 *E* and *F*).

Papaverine Reduces Tumor Hypoxia and Enhances Response to Radiation Therapy. Our model predicts that decreasing oxygen consumption within a tumor will increase overall oxygenation. Therefore, we examined the effect of PPV on partial oxygen pressure (pO_2) in transplanted tumors in mice in real time, using frequency domain near-infrared optical spectroscopy (FD-NIRS), which calculates the pO_2 of the tissue in its light path, using the oxy versus deoxyyhemoglobin ratio and the hemoglobin dissociation curve (23). In heterotopic flank tumors, FD-NIRS shows the baseline pO_2 levels were significantly lower than the same animal's normal thigh muscle (Fig. 2*A*). After establishing a stable baseline pO_2, we delivered either saline or PPV 2 mg/kg in saline to the mouse by tail vein. Five pO_2 traces averaged together show that PPV treatment significantly increased the pO_2 of both the breast and lung tumor models within the first 30–45 min, while saline-treated tumors and PPV-treated thigh muscle showed no significant change (Fig. 2 *B* and *C*). In addition, the duration of the effect was consistent with the expected half-life of PPV, between 90–120 min (24). FD-NIRS data calculate blood pO_2 as an estimate of tissue pO_2, so we further confirmed these findings with the classical hypoxic marker drug pimonidazole to show actual levels of hypoxia in the tumor cells (25). PPV given to tumor-bearing mice 30 min before pimonidazole caused a significant 72% decrease in the hypoxic fraction (pimonidazole positive) of heterotopic EO771 tumors (Fig. 2 *D* and *E*).

Before testing PPV for radiosensitization of tumors, we tested it for inherent radiosensitizing activity. In vitro experiments showed no effect of PPV on the surviving fraction of cells irradiated in either normoxia or hypoxia (*SI Appendix*, Fig. S2 *A* and *B*). Therefore, if we detect potentiation of radiation in vivo, it must be through some secondary effect, like changing the level of tumor oxygenation.

With this in mind, we evaluated the effect of local radiation therapy and/or PPV treatment on model tumor growth (Fig. 2*F*). In orthotopic EO771 mammary tumors in mice, a single dose of PPV had no significant effect, but PPV treatment followed 30 min later by radiation therapy (XRT) produced a significant two- to fourfold enhancement of tumor growth delay over XRT

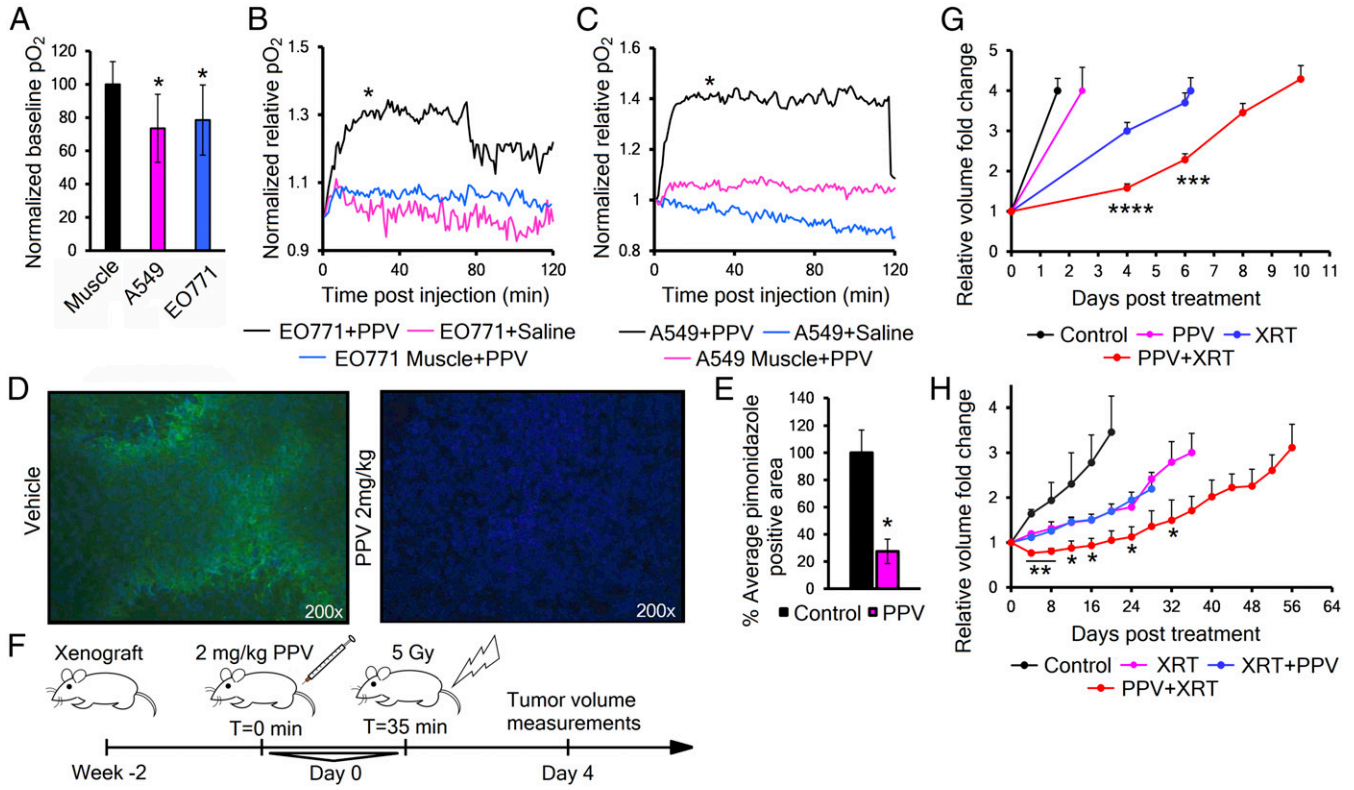

Fig. 2. Papaverine reduces tumor hypoxia and enhances response to radiation therapy. (*A*) FD-NIRS analysis of baseline partial oxygen pressure (pO_2) levels in immune-deficient mice with A549 or EO771 flank xenografts ($n = 3–5$). *P* values were calculated against thigh muscle. (*B* and *C*) Normalized tissue pO_2 in EO771 (*B*) or A549 (*C*) tumor-bearing mice ($n = 5$) after injection of 2 mg/kg PPV or saline (readings taken every minute, and curve is average of five traces). *P* value was analyzed by a linear mixed model with autoregressive correlation structure at T = 30–40 min. (*D*) Representative immunofluorescence image showing pimonidazole (*green*) and Hoechst nuclear counterstain (*blue*) in tumor cryosections from EO771 tumors treated with saline or 2 mg/kg PPV. (*E*) Quantification of hypoxic fractions in *D* ($n = 4$). Values are mean pimonidazole positive area evaluated from 20 images per animal ± SEM. *P* value was calculated with two-tailed two-sample *t* test. (*F*) Schematic of the PPV+XRT experimental design. (*G*) Quantification of tumor growth delay of orthotopic EO771 tumors grown in nude mice receiving either 2 mg/kg PPV (*magenta*), 5 Gy XRT (*blue*) or 2 mg/kg PPV 35 min before 5 Gy XRT (*red*) ($n = 9–10$). Curves represent mean tumor volumes ± SEM. *P* values were calculated against XRT by *t* test. (*H*) Tumor growth of heterotopic A549 flank xenografts in nude mice receiving either 8 Gy XRT (*magenta*), 2 mg/kg PPV 35 min after (*blue*) or before (*red*) 8 Gy XRT ($n = 6$). Error bars are ±SEM. *P* values were calculated against XRT by *t* test. **P* < 0.05; ***P* < 0.01; ****P* < 0.001; *****P* < 0.0001.

alone (Fig. 2*G* and *SI Appendix*, Fig. S2*C*). Interestingly, in heterotopic A549 lung tumors, PPV treatment before XRT showed a similar effect, but treatment with PPV after XRT did not have any effect compared with radiation alone (Fig. 2*H* and *SI Appendix*, Fig. S2*D*). We interpret these findings to indicate that PPV must affect the tumor metabolism before XRT to achieve radiosensitization.

The therapeutic index in radiation oncology is defined by the ability to achieve tumor control versus the production of normal tissue toxicity. Therefore, we next investigated whether PPV increases radiation-induced cell death in normal tissue using the GI crypt assay. Wild-type mice received vehicle, PPV alone, 7.5 Gy total abdominal radiation or PPV followed 30 min later by whole-abdomen irradiation. Groups of animals were killed 1 or 3 d later and the jejunum analyzed for intestinal crypt number and proliferation (Fig. 3*A*). Consistent with our model, PPV did not exacerbate radiation-induced death of normal crypt cells at 24 h or prevent regeneration at 72 h. Surprisingly, there may even be a modest radioprotective effect (Fig. 3 *B* and *C*). Reversal of hypoxia could potentially radiosensitize normal tissue with low oxygen tension. Several normal tissues are reported to contain low-oxygen regions, so we checked to see if murine small intestine was hypoxic. Consistent with the literature (26), we found that normal mouse intestinal epithelia stains with pimonidazole, and there appears a modest reduction in this staining after treatment with papaverine (Fig. 3*D*). We interpret these results to show normal GI tissue has modest physiological hypoxia, but it is not radiosensitized by papaverine, perhaps because this level of hypoxia is not severe enough to radioprotect.

Papaverine Radiosensitizes Through Complex I Inhibition. To mechanistically establish that PPV is radiosensitizing through inhibition of mitochondrial complex I, we engineered cells with PPV-resistant mitochondria. We used CRISPR/Cas9 to remove the essential complex I subunit NDUFV1 (27) and then introduced the rotenone-resistant yeast complex 1 paralog NDI1 into A549 cells (Fig. 4*A* and *SI Appendix*, Fig. S3 *A* and *B*). Previous reports have shown that NDI1 can restore partial mammalian complex I function (28) (*SI Appendix*, Fig. S3*C*). We confirmed that NDI1 rescued mitochondrial function in the NDUFV1 KO cells by showing it could support cell survival in media with only galactose as an energy source (Fig. 4*B*). Further analysis by Seahorse revealed that NDUFV1 KO, NDI1-expressing cells had mitochondria that were resistant to both PPV and rotenone (Fig. 4*C*). Cells with papaverine-resistant mitochondria were then used to grow tumors in mice to test for PPV-dependent effects in vivo. Tumor-bearing mice were treated with PPV, followed by pimonidazole. Staining of sections showed no decrease of the hypoxic fraction (Fig. 4*D*). A second set of tumor-bearing animals were treated with either radiation or PPV followed by radiation. Fig. 4*E* shows these tumors are

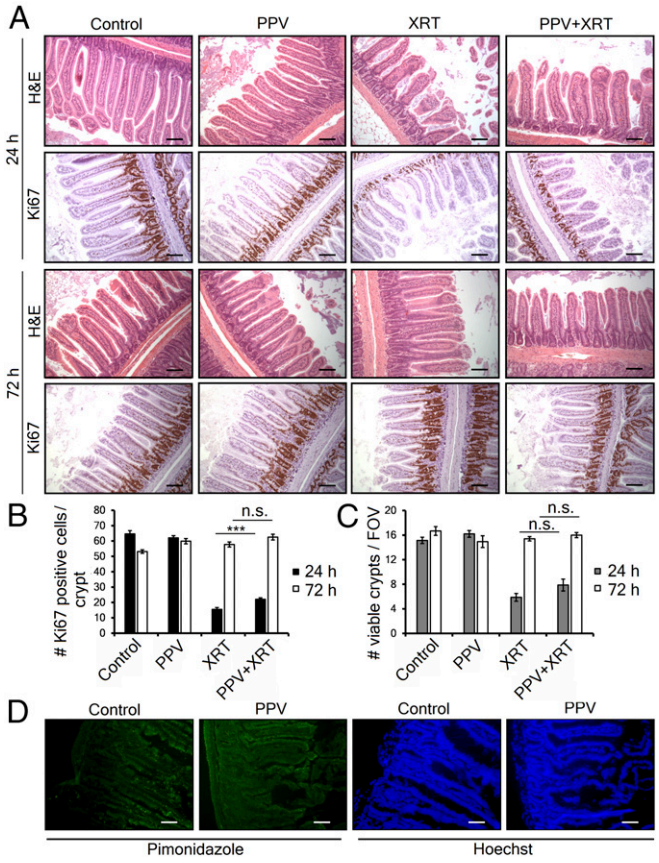

Fig. 3. Papaverine does not increase radiation-induced normal tissue toxicity. (*A*) Representative H&E- and Ki67-stained sections of jejunum harvested 24 or 72 h after treatment with papaverine and/or radiation as indicated. (Scale bar, 100 μm.) (*B*) Quantification of proliferating cells/crypt by Ki67 staining. Data represent mean of at least 30 counted crypts per group (n = 3) ±SEM. (*C*) The number of regenerating crypts/field of view (FOV). Values represent the mean number of crypts with >10 Ki67-positive cells per FOV ±SEM. *P* values were calculated with *t* test. ***$P < 0.001$; n.s., not significant. (*D*) Immunofluorescence showing hypoxic marker pimonidazole (*green*) and Hoechst nuclear counterstain (*blue*) in jejunum cryosections from MiaPaca-2 tumor-bearing mice treated with saline or 2 mg/kg PPV (n = 4). (Scale bar, 50 μm.)

resistant to PPV-dependent increase in radiation growth delay, confirming that PPV radiosensitizes tumors through inhibition of complex I (Fig. 4*E* and *SI Appendix*, Fig. S3*E*).

Papaverine Can Be Reengineered to Remove PDE-Inhibiting Activity. PPV has a long history of clinical use as a treatment of cerebral and peripheral arterial spasm due to its activity as a phosphodiesterase 10A (PDE10A) inhibitor (29). However, in vitro treatment of cells with other PDE inhibitors or 8-Br-cAMP showed no decrease in OCR, indicating that elevated cAMP was not responsible for its mitochondrial effects (*SI Appendix*, Fig. S4 *A* and *B*). Therefore, we reengineered the PPV molecule to separate the PDE activity from the mitochondrial activity. These derivatives could support the model of PPV radiosensitization and remove unwanted activity that might result in potential side effects. Analysis of 41 lead derivatives of PPV identified two lead compounds, SMV-23 and SMV-32, that have separated the OCR and PDE inhibition activity by over 10-fold in vitro (Fig. 5 *A*–*C* and *SI Appendix*, Fig. S4*C* and Table S2). By Seahorse analysis and PDE10A enzymatic assay, we determined that SMV-23 has a mitochondrial IC50 of 94 μM and PDE IC20 of 0.5 μM, while SMV-32 has a mitochondrial IC50 of 7.2 μM and PDE IC20 of 13.42 μM (Fig. 5 *B* and *C*). Next, we determined that SMV-32 dose-dependently blocks the effect of rotenone, suggesting that SMV-32 is capable of binding to complex I similar to the parent molecule (*SI Appendix*, Fig. S4*D*). Neither of these compounds shows cellular toxicity at 10 μM in vitro (*SI Appendix*, Fig. S4*E*), but we needed to determine if either of these compounds was any safer than the parent molecule. PPV has a high rodent LD50 when delivered slowly, but it can be toxic when delivered quickly because it acutely decreases vascular compliance, leading to cardiovascular collapse. We find that in isoflurane-anesthetized mice a rapid dose of 6 mg/kg PPV is toxic. However, neither of the two lead derivatives showed toxicity at this dose and infusion rate, suggesting that the combination of PDE and mitochondrial activities resulted in PPV toxicity (Fig. 5*D*). In vivo, SMV-32 decreased tumor hypoxia by pimonidazole staining, while SMV-23 had no effect on the hypoxic fraction (Fig. 5*E*). Finally, these molecules were compared with the parent molecule for radiosensitization of tumors. In heterotopic EO771 and A549 tumors, SMV-23 shows no increase in growth delay compared with radiation alone, while SMV-32 shows activity that is comparable to papaverine (Fig. 5 *F* and *G*).

Discussion

"Metabolic radiosensitization" is a therapeutic concept that targets the metabolic demand for oxygen by downregulating mitochondrial oxidative metabolism. Previous work has shown that decreasing oxygen consumption in the cores of 3D tumor spheroids decreases the level of hypoxia that displays radiation resistance (12). Our data now show that a single dose of a safe, FDA-approved drug papaverine (PPV) inhibits mitochondrial electron transport chain complex I and transiently reduces tumor

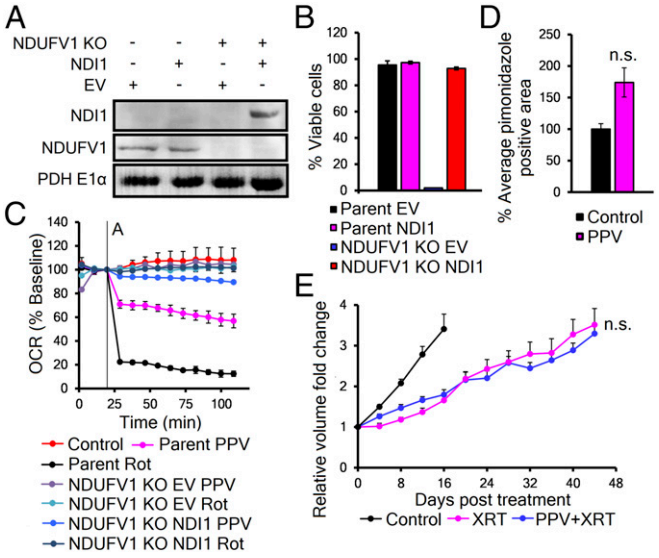

Fig. 4. Papaverine radiosensitizes through complex I inhibition. (*A*) Western blot of NDI1 expression in mitochondrial fractions of parent A549 and NDUFV1 KO cells. (*B*) Representative trypan blue viability (n = 3) of cells grown in galactose-only media (T = 96 h). Values represent mean viable cells ± SD. (*C*) Seahorse analysis of the response of parent A549 and NDUFV1 KO ± NDI1 cells to 10 μM papaverine or 1 μM rotenone. Values are mean ± SD. (*D*) Quantification of pimonidazole staining in NDUFV1 KO NDI1 flank tumors treated with 2 mg/kg PPV or vehicle (n = 3). Value is mean pimonidazole-positive cells from 20 images per tumor ± SEM. *P* value was calculated with *t* test. (*E*) Quantification of tumor growth delay of heterotopic NDUFV1 KO NDI1 flank xenografts receiving either 8 Gy XRT (*magenta*) or 2 mg/kg PPV 35 min before 8 Gy XRT (blue) (n = 4). Curves represent mean tumor volumes ± SEM. *P* values were calculated against XRT with *t* test. n.s., not significant.

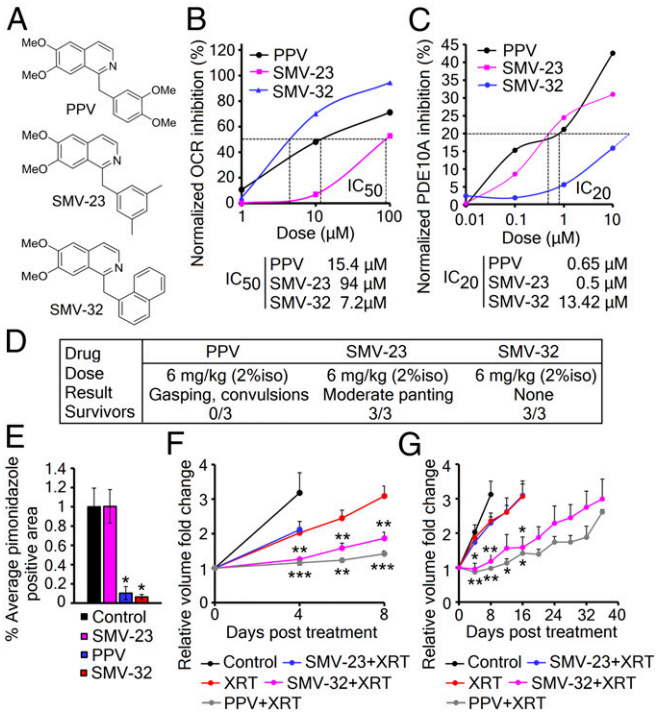

Fig. 5. Papaverine can be reengineered to remove PDE activity. (*A*) Structures of papaverine and the lead derivatives SMV-23 and SMV-32. (*B*) Calculation of OCR IC50 in A549 cells by Seahorse, $n = 5$ replicates per group. (*C*) Calculation of PDE10A IC20 by PDE10A enzymatic assay; $n = 3$ replicates per group. (*D*) Acute toxicity in wild-type C57BL/6 mice ($n = 3$). (*E*) Quantification of hypoxic fractions in orthotopic EO771 tumors treated with 2 mg/kg PPV, SMV-23, SMV-32, or vehicle ($n = 3$). Bar graphs represent the mean area of pimonidazole-positive cells from 20 images per animal ± SEM. *P* value was calculated against control by *t* test. (*F*) Tumor growth delay of heterotopic EO771 flank tumors in nude mice receiving either 5 Gy XRT (*red*) or 2 mg/kg SMV-23 (*blue*), or SMV-32 (*magenta*) or PPV (*gray*) 35 min before 5 Gy XRT ($n = 8$). (*G*) Tumor growth delay of heterotopic A549 flank tumors in nude mice receiving either 8 Gy XRT (*red*) or 2 mg/kg SMV-23 (*blue*), or SMV-32 (*magenta*) or PPV (*gray*) 35 min before 8 Gy XRT ($n = 5$–6). Mean volumes ± SEM. *P* values were calculated against XRT with *t* test. $*P < 0.05$; $**P < 0.01$; $***P < 0.001$.

hypoxia, providing a clinically manageable therapeutic window to deliver more effective radiation therapy.

We identified that PPV is a dual-activity drug independently inhibiting mitochondrial OCR and phosphodiesterase 10 (PDE10A) activity that mediates vasodilation. This raises a question whether both activities contribute to the radiosensitization effect. Previous reports have suggested using vasodilators to enhance radiotherapeutic response (30, 31). However, it has been shown that vasodilator-mediated increase in normal-tissue blood flow reduces tumor perfusion in a process known as vascular steal (32). Due to this and partially because of limited functionality and lack of muscular tone of the tumor vessels, vasodilation has not proven to be effective clinically (33). By generating cancer models with papaverine-resistant mitochondria and PPV derivatives with separated inhibitory activities, we confirmed that PPV achieves radiosensitization exclusively by its effect on mitochondrial function in the tumor cell.

In radiation oncology, clinical doses are determined by the tolerance of the adjacent normal tissue. Therefore, for clinical utility, radiosensitizers must have some specificity for the tumor. Hypoxia is limited to the tumor, so it represents an ideal target for tumor specific radiosensitization. However, the oxygen enhancement effect is not a linear function. Most tissue is at near-maximal radiation sensitivity at ~2% oxygen. Therefore, normal tissue is already at maximal radiosensitivity, and any increase in oxygenation will not result in added radiation toxicity, as we determined in the normal GI tract. These results also indicate that papaverine is not an inherent radiosensitizer and must function through secondary effects.

Preclinical strategies to radiosensitize tumors have failed to translate into clinical practice for a number of reasons. Other molecules currently proposed for metabolic radiosensitization have their caveats, such as a requirement for a week-long pretreatment to achieve OCR reductions (34), transporter-dependent drug uptake that limits the application only to cancer types with high expression of the organic cation transports (35), or a mitochondrial inhibitory effect that is not reversible, leading to safety concerns and overdose potential (36). We show that PPV, on the other hand, is cell-permeable, reversible, and quickly cleared from the patient. In addition, all 28 tested cell lines were sensitive to PPV regardless of their oncogenic landscape, suggesting possible application for a broad spectrum of cancers that depends primarily on their level of hypoxia. It is possible that some oncogenic changes that influence metabolism and mitochondrial function, such as loss of p53 (37) or myc activation (38), can influence the tumor OCR and the potential utility of papaverine as a radiosensitizer.

PPV's dosing has been refined over 100 y of use with a well-established safety profile. Importantly, for radiosensitization, PPV only requires a single dose 45 min before radiation therapy. The drug is cleared rapidly, so that dosing can be repeated daily during conventional fractionation or hypofractionated radiation protocols.

To conclude, PPV or one of its derivatives appear to be ideal candidates for clinical radiosensitization. We believe the added benefit of papaverine in combination with stereotactic beam radiation therapy (SBRT) would be applicable in cancers where local control increases the overall survival. Larger dose per fraction protocols would theoretically see the biggest impact of a reduction in the resistant hypoxic cell fraction because the normoxic and hypoxic radiation survival curves diverge widely at higher doses. The key to the use of such a radiosensitizer will be identifying those tumors with significant hypoxia that would be predicted to benefit from this targeted therapy.

Methods

Cell Lines. All cell lines were purchased from the American Type Culture Collection (ATCC) and grown in DMEM (Corning) supplemented with 10% FBS (Seradigm) and 1% Pen/Strep (Fisher Bioreagents). Cells were treated with inhibitors papaverine hydrochloride (Sigma-Aldrich), rotenone (Sigma-Aldrich), piericidin A (Santa Cruz), capsaicin (Sigma-Aldrich), antimycin A (Sigma-Aldrich), and succinic acid disodium salt (Sigma-Aldrich). Cell viability was assessed by trypan blue exclusion.

CRISPR/Cas9 Genetic Knockout of NDUFV1. Three separate human NDUFV1 guide RNAs (gRNAs) were obtained from GenScript (catalog no. SC1678, item no. U5053CH250_1-3). Lentiviruses were produced by cotransfection of HEK293T cell line with envelope and packaging vectors (delta 8.2 and VSV G2). Virus-containing media were collected after 48 h, and A549 cells were infected in the presence of 8 μg/mL Polybrene (Millipore). After 72 h of selection in 1 μg/mL Puromycin (Sigma-Aldrich) the cells were diluted into single-cell suspensions, and individual clones were screened for compromised OCR by Seahorse. NDUFV1 knockout was confirmed by immunoblotting of mitochondrial fraction of candidate A549 clones.

Seahorse Analysis of the OCR. Oxygen consumption rate (OCR) was measured using Seahorse XF96 (Agilent Technologies). The cells were seeded overnight, washed with prewarmed XF Calibrant, and replaced with unbuffered Assay Medium (pH 7.4, 5 mM glucose, 1 mM L-glutamine) and incubated 2 h. For succinate rescue assay, cells were permeabilized using XF Plasma Membrane Permeabilizer Reagent according to the manufacturer's instructions. The OCR rate was measured in 1× Mitochondrial Assay Solution (MAS) [70 mM sucrose, 220 mM mannitol, 10 mM KH_2PO_4, 5 mM $MgCl_2$, 2 mM Hepes, 0.6% (wt/vol) fatty acid-free BSA, and 1 mM EGTA; pH 7.4]. After baseline oxygenation was established, 1 μM rotenone or 10 μM PPV was injected at time

A, followed by 5 mM succinate at time B. For the washout experiment, EO771 cells were treated with 10 μM PPV or 1 μM rotenone 3 h before OCR measurement. Media was replaced 1 and 2 h before measurement, and OCR was reported.

In Vivo Partial Oxygen Pressure Measurements. All animal experiments were performed according to protocols approved by institutional IACUC review, with daily veterinarian observation. The 2×10^6 EO771 or 5×10^6 A549 cells were injected s.c. into the flanks of 6-wk-old female immunocompromised nu/nu mice. Caliper measurements of opposing diameters were used to calculate the tumor volumes. Upon reaching 500 mm^3, the animals were anesthetized by inhalation of 1.5% isoflurane, and tumor and thigh muscle partial oxygen pressure (pO_2) was measured with NIRS optical probe for 30 min. pO2 was established using custom-built frequency-domain photon migration (FDPM) instrument, described in detail in ref. 23. Briefly, we used a six-wavelength (654, 683, 779, 805, 847, and 905 nm) FDPM instrument with a side-firing optical probe consisting of two side-firing source fibers and a single side-firing detection fiber attached to a thin Delrin plate to generate a flat surface probe that can be placed on top of a rodent model tumor. Two source detector separations were used to reduce skin absorption effects as well as to eliminate instrumentation drifts or artifacts. The concentrations of oxy- and deoxy-hemoglobin (HbO and HbR, respectively) were determined by analyzing the reflectance spectra using custom LabVIEW program integrated with Matlab scripts. pO_2 was calculated as follows: $pO_2 = HbO/THC$ (total hemoglobin concentration), where $THC = HbO + HbR$. The penetration depth, and thus the sample volume, was estimated to be 5–15 mm in model tumors. Once the baseline oxygenation was established, the animals were injected with either 2 mg per kg of body weight of papaverine hydrochloride or saline by tail vein. Tissue oxygenation was measured for 120 min. Obtained oxygenation values were normalized to time of injection and represent the average of three to five traces per treatment.

Pimonidazole Staining. Pimonidazole adducts were visualized in hypoxic regions within histological sections of tumor tissues (39). Mice bearing EO771 and A549 flank xenografts were treated with 2 mg/kg PPV or saline and, 30 min later, 60 mg/kg pimonidazole i.p., and tumors were harvested at 90 min. Frozen sections were stained with anti-pimonidazole rabbit antibody and anti-rabbit Alexa Fluor 488. The hypoxic fraction of each tumor was quantified by thresholding signal at 50% of the maximum signal on control sections. The area covered by pimonidazole-positive cells was evaluated from 20 images per animal and averaged.

Tumor Growth Kinetics. The 2×10^6 EO771 or 5×10^6 A549 cells were injected s.c. into the flanks of 6-wk-old female immunocompetent C57/B6 (EO771) or immunocompromised nu/nu (A549) mice. Caliper measurements of opposing diameter were used to calculate the tumor volumes. Upon reaching 150 mm^3, the tumors were visualized by cone beam CT, and treatment plans were calculated using SARRP software. X-rays were delivered with a single beam delivering 5 Gy using the Small Animal Research Radiation Platform (SARRP; Xstrahl). Tumor volumes were measured until the posttreatment volume increased threefold.

Intestinal Crypt Assay. Wild-type C57/B6 mice received abdominal 7.5 Gy dose of XRT delivered using the SARRP. Dissected small intestines were fixed with 10% natural-buffered formalin (NBF) before being embedded in paraffin. Anti-Ki67 antibody (Thermo Scientific RM-9106-S) was detected by Vector Laboratories goat anti-rabbit (DAB chromagen).

ACKNOWLEDGMENTS. We thank Kyle Porter for his statistical input and Navdeep Chandel for the NDI1 expression plasmid. Funding was provided by Grants NIH P01CA016776 and R01CA163581.

1. Brown JM, Giaccia AJ (1998) The unique physiology of solid tumors: Opportunities (and problems) for cancer therapy. *Cancer Res* 58:1408–1416.
2. Epstein T, Xu L, Gillies RJ, Gatenby RA (2014) Separation of metabolic supply and demand: Aerobic glycolysis as a normal physiological response to fluctuating energetic demands in the membrane. *Cancer Metab* 2:7.
3. Semenza GL (2013) HIF-1 mediates metabolic responses to intratumoral hypoxia and oncogenic mutations. *J Clin Invest* 123:3664–3671.
4. Harrison DK, Vaupel P (2014) Heterogeneity in tissue oxygenation: From physiological variability in normal tissues to pathophysiological chaos in malignant tumours. *Adv Exp Med Biol* 812:25–31.
5. Thomlinson RH, Gray LH (1955) The histological structure of some human lung cancers and the possible implications for radiotherapy. *Br J Cancer* 9:539–549.
6. Baskar R, Lee KA, Yeo R, Yeoh K-W (2012) Cancer and radiation therapy: Current advances and future directions. *Int J Med Sci* 9:193–199.
7. Prise KM, Gillies NE, Michael BD (1998) Evidence for a hypoxic fixation reaction leading to the induction of ssb and dsb in irradiated DNA. *Int J Radiat Biol* 74:53–59.
8. Johansen I, Howard-Flanders P (1965) Macromolecular repair and free radical scavenging in the protection of bacteria against X-rays. *Radiat Res* 24:184–200.
9. Freyer JP, Jarrett K, Carpenter S, Raju MR (1991) Oxygen enhancement ratio as a function of dose and cell cycle phase for radiation-resistant and sensitive CHO cells. *Radiat Res* 127:297–307.
10. Siemann DW, Alliet KL, Macler LM (1989) Manipulations in the oxygen transport capacity of blood as a means of sensitizing tumors to radiation therapy. *Int J Radiat Oncol Biol Phys* 16:1169–1172.
11. Saunders M, Dische S (1996) Clinical results of hypoxic cell radiosensitisation from hyperbaric oxygen to accelerated radiotherapy, carbogen and nicotinamide. *Br J Cancer Suppl* 27:S271–S278.
12. Secomb TW, Hsu R, Ong ET, Gross JF, Dewhirst MW (1995) Analysis of the effects of oxygen supply and demand on hypoxic fraction in tumors. *Acta Oncol* 34:313–316.
13. Secomb TW, Hsu R, Dewhirst MW (2004) Synergistic effects of hyperoxic gas breathing and reduced oxygen consumption on tumor oxygenation: A theoretical model. *Int J Radiat Oncol Biol Phys* 59:572–578.
14. Ashton TM, McKenna WG, Kunz-Schughart LA, Higgins GS (2018) Oxidative phosphorylation as an emerging target in cancer therapy. *Clin Cancer Res* 24:2482–2490.
15. De Takats G (1970) Papaverine: Use and toxicity. *N Engl J Med* 282:225.
16. Merck G (1848) Vorläufige Notiz über eine neue organische Base im Opium. *Ann Chem Pharm* 66:125–128.
17. Liu HM, Tu YK (2002) The efficacy of papaverine administration by different routes for the treatment of experimental acute cerebral vasospasm. *J Clin Neurosci* 9:561–565.
18. Yildiz N, Gokkaya NK, Koseoglu F, Gokkaya S, Comert D (2011) Efficacies of papaverine and sildenafil in the treatment of erectile dysfunction in early-stage paraplegic men. *Int J Rehabil Res* 34:44–52.
19. Chappie TA, et al. (2007) Discovery of a series of 6,7-dimethoxy-4-pyrrolidylquinazoline PDE10A inhibitors. *J Med Chem* 50:182–185.
20. Gohil VM, et al. (2010) Nutrient-sensitized screening for drugs that shift energy metabolism from mitochondrial respiration to glycolysis. *Nat Biotechnol* 28:249–255.
21. Morikawa N, Nakagawa-Hattori Y, Mizuno Y (1996) Effect of dopamine, dimethoxyphenylethylamine, papaverine, and related compounds on mitochondrial respiration and complex I activity. *J Neurochem* 66:1174–1181.
22. Xiong N, et al. (2012) Mitochondrial complex I inhibitor rotenone-induced toxicity and its potential mechanisms in Parkinson's disease models. *Crit Rev Toxicol* 42:613–632.
23. Yu B, et al. (2014) Measuring tumor cycling hypoxia and angiogenesis using a side-firing fiber optic probe. *J Biophotonics* 7:552–564.
24. Ritschel WA, Hammer GV (1977) Pharmacokinetics of papaverine in man. *Int J Clin Pharmacol Biopharm* 15:227–228.
25. Rademakers SE, Lok J, van der Kogel AJ, Bussink J, Kaanders JH (2011) Metabolic markers in relation to hypoxia; staining patterns and colocalization of pimonidazole, HIF-1α, CAIX, LDH-5, GLUT-1, MCT1 and MCT4. *BMC Cancer* 11:167.
26. Zheng L, Kelly CJ, Colgan SP (2015) Physiologic hypoxia and oxygen homeostasis in the healthy intestine. A review in the theme: Cellular responses to hypoxia. *Am J Physiol Cell Physiol* 309:C350–C360.
27. Bénit P, et al. (2001) Large-scale deletion and point mutations of the nuclear NDUFV1 and NDUFS1 genes in mitochondrial complex I deficiency. *Am J Hum Genet* 68:1344–1352.
28. Seo BB, et al. (1998) Molecular remedy of complex I defects: Rotenone-insensitive internal NADH-quinone oxidoreductase of Saccharomyces cerevisiae mitochondria restores the NADH oxidase activity of complex I-deficient mammalian cells. *Proc Natl Acad Sci USA* 95:9167–9171.
29. Gagnon G, Regoli D, Rioux F (1980) Studies on the mechanism of action of various vasodilators. *Br J Pharmacol* 70:219–227.
30. Abramovic Z, et al. (2011) Modulation of tumor hypoxia by topical formulations with vasodilators for enhancing therapy. *Adv Exp Med Biol* 701:75–82.
31. De Ridder M, Verellen D, Verovski V, Storme G (2008) Hypoxic tumor cell radiosensitization through nitric oxide. *Nitric Oxide* 19:164–169.
32. Shan SQ, et al. (1997) Effects of diethylamine/nitric oxide on blood perfusion and oxygenation in the R3230Ac mammary carcinoma. *Br J Cancer* 76:429–437.
33. Vaupel P (2004) Tumor microenvironmental physiology and its implications for radiation oncology. *Semin Radiat Oncol* 14:198–206.
34. Ashton TM, et al. (2016) The anti-malarial atovaquone increases radiosensitivity by alleviating tumour hypoxia. *Nat Commun* 7:12308.
35. Wheaton WW, et al. (2014) Metformin inhibits mitochondrial complex I of cancer cells to reduce tumorigenesis. *eLife* 3:e02242.
36. Ellinghaus P, et al. (2013) BAY 87-2243, a highly potent and selective inhibitor of hypoxia-induced gene activation has antitumor activities by inhibition of mitochondrial complex I. *Cancer Med* 2:611–624.
37. Matoba S, et al. (2006) p53 regulates mitochondrial respiration. *Science* 312:1650–1653.
38. Gao P, et al. (2009) c-Myc suppression of miR-23a/b enhances mitochondrial glutaminase expression and glutamine metabolism. *Nature* 458:762–765.
39. Kizaka-Kondoh S, Konse-Nagasawa H (2009) Significance of nitroimidazole compounds and hypoxia-inducible factor-1 for imaging tumor hypoxia. *Cancer Sci* 100:1366–1373.